Journal of Applied Chemical Research

jacr.kiau.ac.ir

Journal of Applied Chemical Research, 15, 3, 88-105(2021)

Synthesis and Investigation of Corrosion Inhibition of 4-(naphthalen-1-yl) thiazol-2-amineoncopper in HCl: Experimental and Theoretical Studies

Razieh Farahati[1],S. Morteza Mousavi-Khoshdel[1*],Ali Ghaffarinejad[1,2,3] , Hamidreza (Jafar) Rezania[4]

[1]Industrial Electrochemistry Research Laboratory, Faculty of Chemistry, Iran University of Science and Technology, Tehran, Iran
[2]Research Laboratory of Real Samples Analysis, Faculty of Chemistry, Iran University of Science and Technology, Tehran, Iran
[3]Electroanalytical Chemistry Research Center, Iran University of Science and Technology, Tehran, Iran
[4]Department of Organic Chemistry, Faculty of Chemistry, Kharazmi University, Tehran, Iran
(Received 15Aug. 2019; Final revised received 19Nov.2019)

Abstract

4-(naphthalen-1-yl) thiazol-2-amine (NTA) was synthesized and its corrosion inhibition ability on the copper was investigated. The inhibition efficiencies were evaluated by electrochemical impedance spectroscopy (EIS), potentiodynamic polarization, scanning electron microscopy (SEM), and atomic force microscopy (AFM).The experiments were performed in various concentrations of NTA in 1 M HCl solution. Computational studies (molecular dynamics (MD) simulation and density functional theory (DFT)) were also executed. The corrosion inhibition efficiency of this compound at optimum concentration was about 90%, demonstrating that NTA is an effective corrosion inhibitor. The adsorption of inhibitor obeyed the Langmuir adsorption model.

Keywords: *Copper, EIS, MD,Corrosion inhibition,Thiazole.*

[*]***Corresponding author***:*S. Morteza Mousavi-Khoshdel, Industrial Electrochemistry Research Laboratory, Faculty of Chemistry, Iran University of Science and Technology, Tehran, Iran. E-mail: mmousavi@iust.ac.ir, Tel: +982177240080, Fax: +982177491204)*

Introduction

Copper and its alloys are extensively used in different industries such as electronic industries, marine industries, heat exchangers, power stations, and cooling towers [1,2]. Since the metallic systems constructed from copper are usually exposed toaggressive medium containing nitrate, chlorideor sulfate [3,4], the protection of copper against corrosion attracted considerable attention[5].

Among the corrosion protection methods, the use of inhibitors is an essential and conventional method. It was revealed that organic compounds containing polar groups, heteroatoms, and heterocycles were commonly used to inhibit corrosion [5–7]. Azole organic compounds such as triazoles, imidazoles, and thiazoles applied as effective corrosion inhibitors [8–10]. Thiazoles are aromatic heterocyclic compounds which have shown pharmacological properties [11–15]. Moreover, thiazoles are susceptible for application as the corrosion inhibitor. Studies showed that some thiazoles were well exhibited corrosion inhibition on the metals [16–20]. Notably, using some thiazoles as copper corrosion inhibitors attracted attentions[6,21–25].Investigations showed that electron-donating groups on aromatic ring cause more efficiency than electron-withdrawing groups [22]. Moreover, the polar group, the situation of the group, and conjugated system are effectual in the corrosion inhibition ability [23].To the best of our knowledge, the NTA (Figure 1) corrosion inhibition on the copper in HCl has been examined in no study yet.In this report, the NTA was synthesized, and its corrosion inhibition on the copper in 1 M HCl wasempirically examined by using electrochemical techniques and surface analysis tests.

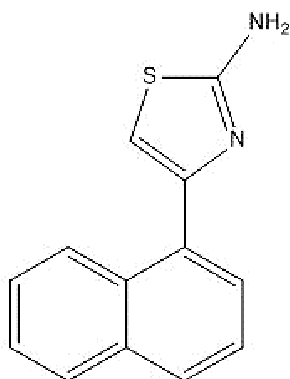

Figure 1. Chemical structure of 4-(naphthalen-1-yl) thiazol-2-amine (NTA).

Experimental

Materials

1-Acetylnaphthalene, thiourea, and diiodine were obtained from Sigma-Aldrich Co., Germany. 4-(naphthalen-1-yl)thiazol-2-amine was synthesizedbased on our modified procedure [26]. HCl

prepared from Merck for providing solutions. The measurements were carried out in stationary 1 M HCl, which was a solution with varying concentrations of NTA(0, 0.1, 0.5, 1,and2 mM). The 3-mm diameter copper rod was coated with epoxy resin and was used as the working electrode.

Synthesis of diamine monomers

The mixtures of 2.53 g (10 mmol) of diiodine, 1.53 g (20 mmol) of thiourea, and 1.70 g (10 mmol) of1-acetylnaphthalene were stirred and heated to melt at 116 °C for 6 h. After reaction mixture becomes solid, the reaction media solved into 200 mL water with heating. The obtained solution filtered and neutralized with a basic solution (sodium hydroxide 1 M) to precipitate. The acquired precipitate was filtered, washed with water, and recrystallized from H_2O/EtOH (1:1) to afford 4-(3-nitrophenyl) thiazol-2-amine. The synthesis procedure of NTA was shown in Figure 2. The characterization of the prepared compound (FTIR and NMR spectra) is available in the supplementary information.

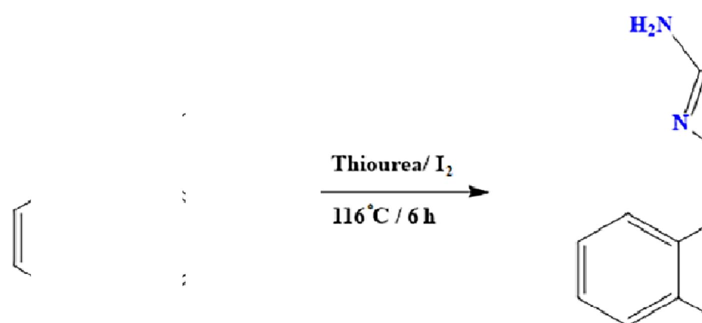

Figure 2. The synthesis procedure of NTA.

Electrochemical studies

All electrochemical tests were executed at room temperature by a Potentiostat/Galvanostat model of PGSTAT 204 (Metrohm Autolab, Netherlands) equipped with Nova 2.1 software. The electrochemical cell was a three-electrode system using Pt rod as a counter electrode, Ag|AgCl|3 M KCl as a reference electrode, and Cu rod as a working electrode. Tafel diagrams were attained in the potential range of -0.4 to 0 $V_{Ag/AgCl}$ with the scan rate of 0.001 $V.s^{-1}$. EIS tests were done at open circuit potential (OCP) with 10 mV amplitude in the frequency of 10^5 to 10^{-1} Hz.

Surface analysis

The copper surfaces were first abraded using sandpapers (grades 600, 1000, and 2000), then rinsed with deionized water, and finally dried and immersed in 1 M HCl solution in the presence and

absence of NTA for 1 h. Then, the specimens were washed with deionized water and dried in Ar stream. Lastly, the micrograph images of sample surfaces were obtained using a scanning electron microscope (TESCAN VEGA2, Czech Republic) and an AFM (Nanoscope scanning probe microscopes digital instruments /USA).

Computational details

Geometry optimizations of the NTA were done by DFT method at the B3LYP level with 6-311++g(d,p) basis set [27–29]. Frequency calculations of optimized structures were executed and verified the true minima on the potential energy surface. These calculations were carried out using the Gaussian 03 software [30]. Since thiazoles can exist in the protonated form in the acidic solution, we also performed calculations on the protonated form of NTA. Moreover, DFT calculations were executed to optimize thegeometry of the inhibitor (in non-protonated and protonated forms) on copper using D mol^3 module of Materials Studio software 6.0 [31]. Calculations were performed on the Cu (111). Cu plane was composed of 4 layers, where 2 bottom-most layers were frozen. Cu (111) was enlarged to a (12 × 12) supercell, and separated by a vacuum layer of 20 Å. Calculations were performed using the generalized gradient approximation(GGA), following the Perdew-BuekeErnzerhof scheme (PBE), for the exchange-correlation functional and the DNP double-numeric basis set. The interactions between the inhibitor molecule and the copper surface were simulated using DFT Semi-Core Pseudo-potentials.The interaction energy (E_{int}) between inhibitor and copper surface was obtained by (Eq. 1):

$$E_{int}=E_{tot} - (E_{sur} + E_{inh})(1)$$

where $E_{tot}$and E_{sur} are the total energy of the simulation system with and without the inhibitor, respectively, and $E_{inh}$is the total energy of the inhibitor. MD simulation was carried out using the Forcite molecular dynamics module of the Materials Studio 6.0 software. The interaction between the copper surface, which was enlarged to a (12 × 12) supercell, and NTA was exerted with the periodic boundary conditions in the simulation box. A vacuum slab of 30 Å height was considered above copper surface to prevents the effect of periodic image of surface above molecule. The condensed phase optimized molecular potentials for atomistic simulation studies (COMPASS) force field was employed[32]. Van der Waals, Non-bonding, and electrostatic interactions were set as atom-based summations using the Ewald summation method and a cutoff radius of 9.50 Å. Cu (111) was composed of 10 layers, where 8 bottom-most layers were frozen. The adsorption system contained Cl^-, H_3O^+ ions, H_2O molecules and inhibitor molecule. The MD simulation performed at 298.0 K using canonical ensemble (NVT) with a time step of 1.0 fs and a simulation time of 1000

ps. The geometry of the system was first optimized; then, the simulation was done. The interaction energy E_{int} between NTA and copper surface was computed using the relation given below[33]:

$$E_{int}=E_{tot}-(E_{sur+sol}+E_{inh+sol})+E_{sol} \quad (2)$$

where E_{tot} is the total energy of the simulation system, $E_{sur+sol}$ and $E_{inh+sol}$ are the total energy of the simulation system without the inhibitor and total energy of inhibitor and solution, respectively; E_{sol} is the total energy of the solution without inhibitor.

Results and discussion

Tafel polarization studies

Tafel polarization tests were exerted and some important parameters were extracted from the polarization curves such as corrosion current density (j_{corr}), corrosion potential (E_{corr}), cathodic and anodic Tafel slopes (β_a, β_c),and inhibition efficiency (IE%). The IE% was obtained by the following formula:

$$\text{IE\%} = \frac{j_{corr} - j_{corr\,(inh)}}{j_{corr}} \times 100 \quad (3)$$

where, j_{corr} and $j_{corr(inh)}$ are corrosion current densities of the system without and with inhibitor, respectively. Figure 3 shows Tafel diagrams curves for copper, after soaking in 1 M HCl without with different concentrations of the NTA for 10 min. After this 10-min period, the open circuit potential (OCP) was stable. The parameters acquired from these plots were exhibited in Table 1. As shown in this table, the highest IE% for NTAwas obtained at the inhibitor concentration of 2mM. If the shift of corrosion potential in the presence of the inhibitor toward the blank solution is less than 85 mV, it seems to be a mixed-type inhibitor [34]. If the shift of E_{corr} in the presence of the inhibitor compared with the blank solution is higher than 85 mV; the inhibitor can beclassified as cathodic or anodic type. In the present study, the shift in E_{corr} values was less than 85 mV, the NTA is a mixed-type inhibitor [35].According to Figure3, in thepresence of NTA, however, significantly affected the cathodic reaction.

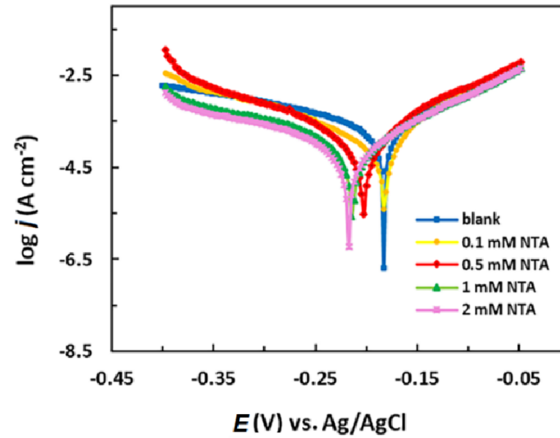

Figure 3. Tafel curves obtained for copper in 1 M HCl solutions without and with various NTA concentrations after a 10-min soaking time

Table 1. Corrosion parameters calculated by polarization curves for copper in 1 M HCl at various NTAinhibitor concentrations.

C_{inh} (mM)	β_a (Vdec^{-1})	β_c (V dec^{-1})	E_{corr} (V)	i_{corr} (μA)	j_{corr}(μA cm^{-2})	IE%$_{Tafel}$
-	0.090	0.174	-0.183	14.54	207.71	-
0.1	0.073	0.056	-0.203	3.96	56.57	72.76
0.5	0.058	0.054	-0.214	2.49	35.57	83.00
1	0.119	0.096	-0.217	2.46	35.14	83.08
2	0.532	0.089	-0.186	2.02	28.86	86.11

Electrochemical impedance spectroscopy (EIS)

The impedance spectra (Figure5) were fitted with the equivalent circuits in Figure 4, Q_1, Q_2, and $W$are Warburg element, constant phase element (CPE) of film or layer of oxide, and CPE of the double layer, respectively. R_s, R_1, and R_2 are the solution resistance, the resistance of the inhibitor film or the oxide layer, and charge transfer resistance, respectively [36]. Circuits (a) and (b) were employed to fit the EIS plots for the copper in 1 M HCl solutions with NTA and copper in the blank, respectively.

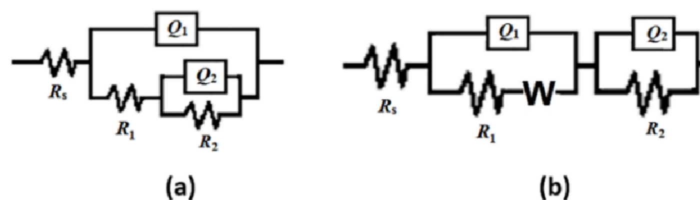

Figure 4. The electrical equivalent circuit was employed for the (a) copper exposure to 1 M HCl solution containing inhibitor and (b) copper exposure to blank.

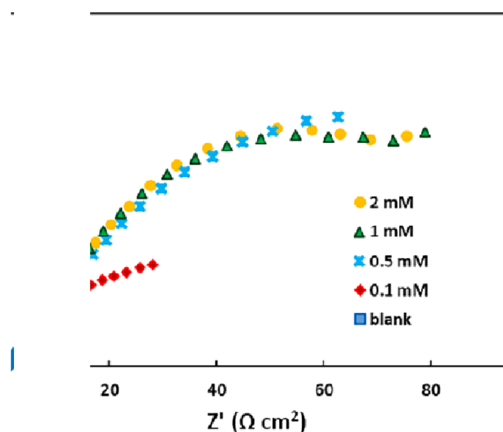

Figure5. Nyquist plots recorded for copper in 1 M HCl solution without and with various NTA concentrations after 10-min soaking time.

Nyquist plots (Figure5) display two incomplete semicircles;(1): a small incomplete loop contributes to the oxide layer or film resistance formed on the surface (R_1) and (2):a large loop associatedwith charge transfer resistance (R_2). From Figure 5, one can observe that in all investigated concentrations, R_1 and R_2 of NTA are more than those of blank. The capacitor behavior can benon-ideal due to the inhibitor adsorption and surface roughness [37].Considering this effect, Q_1 and Q_2 used instead of capacitors. The corrosion products diffusion into the bulk solution or corrosive agents diffusion to thecopper surface causes the Warburg impedance [38,39]. The Warburg impedance was removed and the radius of the loops was increased significantly by addition of the inhibitors to the blank solution, indicating that the inhibitors form a protective layer on the copper surface and inhibit the diffusion of corrosion products to the bulk solution or the diffusion of Cl^- to the copper electrode surface [40–42]. The electrochemical parameters obtained from EIS test are demonstrated in Table 2, where the IE% was calculated by (Eq. 4)[43]:

$$IE\% = \frac{R_{p(inh)} - R_p}{R_{p(inh)}} \times 100 \quad (4)$$

where $R_{p(inh)}$ and R_p are the polarization resistances in the inhibited and uninhibited system, respectively and R_p is equivalent to R_1 + R_2.Double layer capacitance (C_{dl}) was given by (Eq. 5)[44]:

$$C_{dl} = Y_0(2\pi f_{max})^{n-1} \quad (5)$$

where, Y_0 and f_{max} are the CPE magnitude and frequency at which the imaginary component of the impedance reaches the maximum value, respectively. In this equation, n is an adjustable factor, $n = \alpha/(\pi/2)$, and α is the phase angle [45].

According to Table2, in all of the most cases, $Q_1$and Q_2 are declined in the presence of the NTAin comparison with the blank. The decrease of Q is due to a decrease in local dielectric constant or the increase of the double layer thickness [44]. Results of EIS test showed that the maximum efficiency in NTA inhibitor was obtained at 1 mM.

Table 2. Electrochemical parameters acquired from EIS test in the different concentrations of the NTA in 1 M HCl after 10min soaking time.

C_{inh}(mM)	R_s (Ω cm^2)	Q_1		R_1(Ωcm^2)	Q_2		R_2 (Ωcm^2)	IE%
		Y_{01}(Ω^{-1}cm^{-2}s^n)	n_1		Y_{02} (Ω^{-1}cm^{-2} s^n)	n_2		
-	0.50	0.006	0.62	0.71	0.019	0.58	10.02	-
0.1	0.27	0.007	0.52	3.06	0.019	0.57	54.29	80.25
0.5	0.26	0.002	0.61	6.06	0.005	0.66	108.29	90.10
1	0.27	0.002	0.61	4.63	0.010	0.56	138.46	92.26
2	0.25	0.005	0.52	9.24	0.003	0.70	119.70	91.04

In Figure6, the phase graph shows two maximums for two time constants of two occurring processes on the surface [46]. The first time constant (Q_1R_1) is related to the film of adsorbed inhibitor, whereas the second time constant (Q_2R_2) is associated with the double layer [47]. The phase angle moved to more negative values in the presence of NTA compared with the blank, representing more adsorbed inhibitors on the surface and increasing the formation of the double layer on the surface toward capacitor behavior [48]. Bod plots in all of the inhibitor concentrations showed an increase in the values of absolute impedance at low frequencies compared with blank solution, indicating the higher protection.

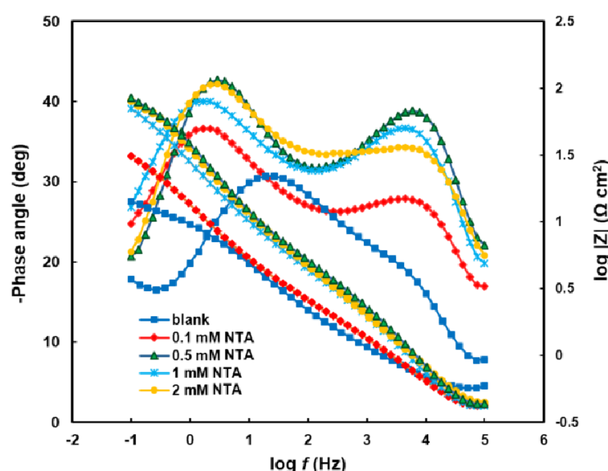

Figure 6. Bode and phase angle plots for copper in 1 M HCl solution in the absence and presence of various NTA concentrations.

AFM observation

AFM is a powerful tool to study the surface morphology and corrosion processes at the metal-solution interface [49]. The AFM 3-dimensional (3D) micrographs of freshly polished Cu, Cu in 1 M HCl/NTA, and Cu in blank solution are shown in Figure7 (a-c), respectively. Observed from this figure that in the inhibited sample, cervices and damages are less than those in the uninhibited sample in 1 M HCl, indicating less corrosion in the presence of inhibitor.

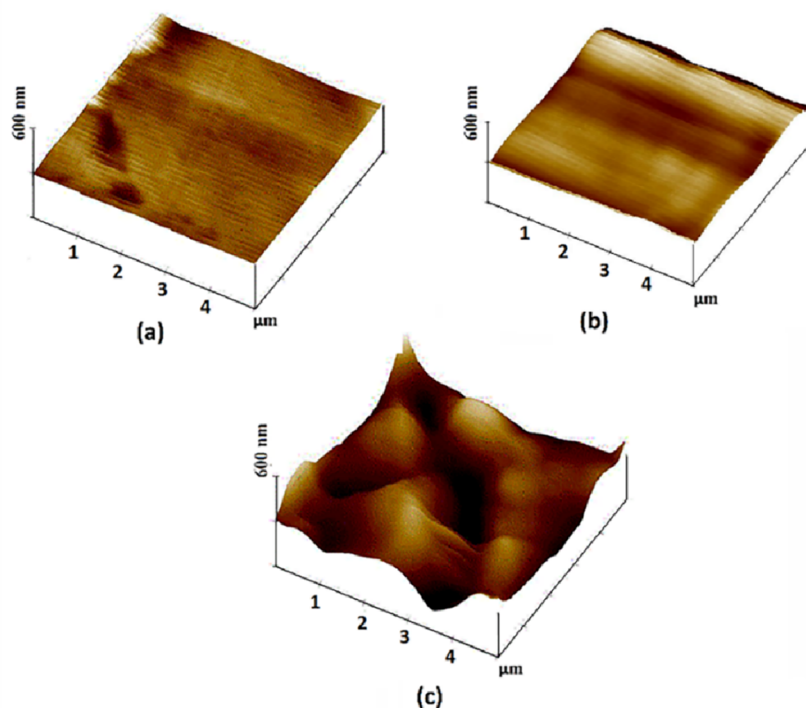

Figure 7. AFM micrographs from the copper surface (a) before and (b) after 1-h soaking time in 1 M HCl+NTA, and (c) Cu in the blank.

SEM analysis

Figure8(a-c) shows the SEM micrographs of copper before and after 1-h soaking time in 1 M HCl in the absence and the presence of optimal inhibitor concentration. It can be observed from Figure8 (b) the copper surface was uniformly pitted in the absence of the inhibitor while the corrosion black holes were noticeably decreased when inhibitor was added.

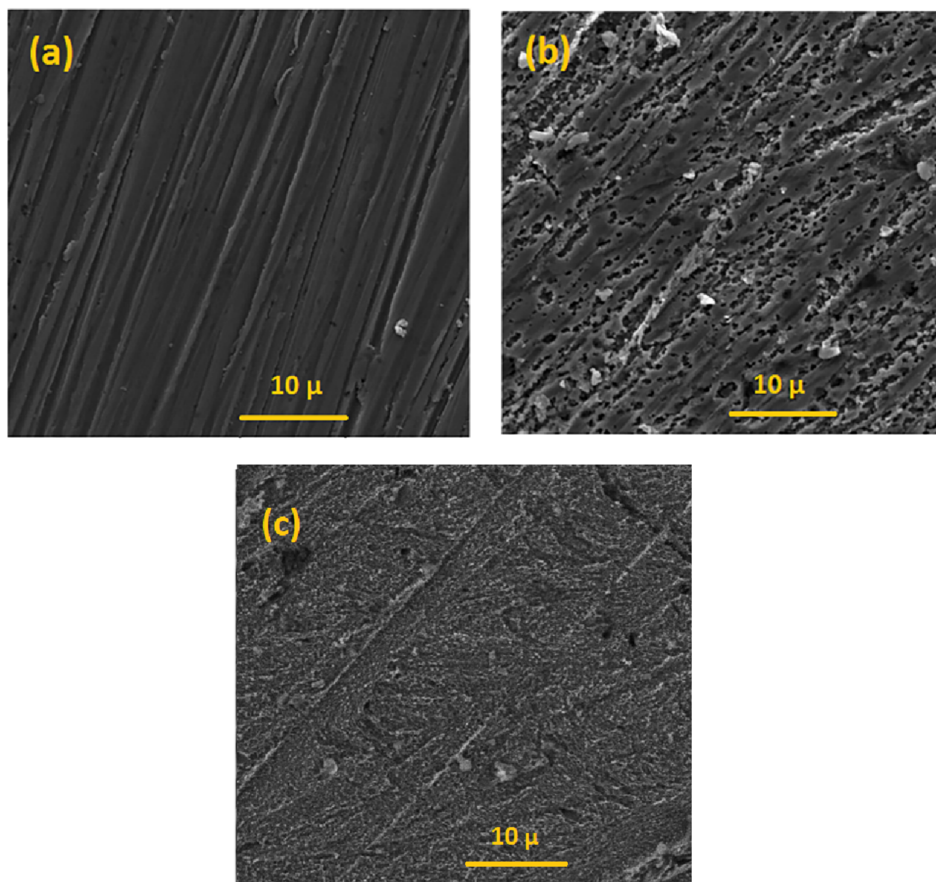

Figure 8. Images were taken by SEM from the copper surface (a) before and (b) after 1-h soaking time in 1 M HCl in the absence and (c)the presence of NTA.

Adsorption isotherm

Commonly, the adsorption of inhibitors can be clarified using adsorption isotherm [50].The corrosion rate generally decreased as there was an increase in the degree of metal surface coverage (θ) with inhibitor molecules. Θ was given by(Eq. 6)[51]:

$$\theta = 10^{-2} \times IE\% \quad (6)$$

The results obtained from electrochemical tests were obeyed the Langmuir adsorption isotherm (Figure9). The Langmuir adsorption isotherm can be described by using(Eq. 7)[50]:

$$\frac{C}{\theta} = \frac{1}{K_{ads}} + C (7)$$

where, K_{ads} is the equilibrium constant for the adsorption process, θ is the surface coverage, and $C$is the concentration of the inhibitor in mM. Free energy of adsorption (ΔG^0_{ads}) was calculated by (Eq. 8)[52]:

$$\Delta G^0_{ads} = -RT\ln(55.5\ K_{ads}) \qquad (8)$$

where, R is the universal gas constant (8.314 J mol^{-1} K^{-1}), and value of 55.5 is the molar concentration of water. The value of ΔG^0_{ads} expresses the nature of the adsorption process such that if ΔG^0_{ads} is less negative than -20 kJ mol^{-1}, the physical adsorption occurs through electrostatic interactions; if ΔG^0_{ads} was more negative than -40 kJ mol^{-1}, the chemical adsorption could occur through electron transfer from inhibitor molecules to the metal; when ΔG^0_{ads} was between -20 and -40 kJ mol^{-1}, both adsorption types could occur [53]. The ΔG^0_{ads} values in Table 3indicate the occurrence of both physical and chemical adsorptions. In other words, both protonated and neutral forms of NTA in the acid solution are adsorbed on the metal surface. The chemisorption could occur through the interaction between π-electrons of aromatic rings or lone-pair electrons of N or S atoms with the copper surface, while the physisorption might happen through electrostatic interaction between the negatively charged surface and positively charged positions of protonated molecules. The negative values of ΔG^0_{ads} indicated spontaneous adsorption of NTA molecules on the copper surface.

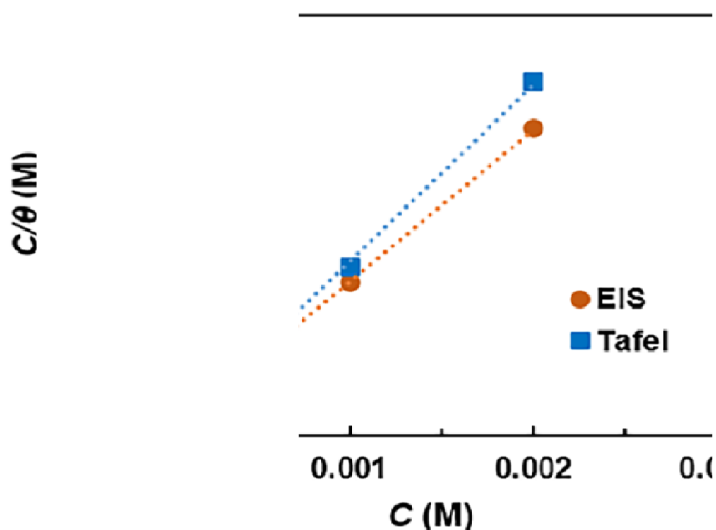

Figure 9. Langmuir adsorption plots of NTA onthe copper in 1 M HCl solution based on EIS and polarization data.

Table 3. Parameters of Langmuir adsorption isotherm for NTAon the copper surface in 1 M HCl based on polarization and EIS data.

Inhibitor type	Technique	r^2	K_{ads} (M^{-1})	ΔG^0_{ads}(kJ mol^{-1})
NTA	Polarization	0.999	63200	-37.36
	EIS	0.999	121233	-38.97

Computational calculations

Quantum chemical calculations were performed on NTA (non-protonated form) and NTA^+ (protonated form) in gas and aqueous phases. To consider the preferred site for the accepting proton, protonation energies of NTA were calculated. Calculations revealed that the most favorable site for protonation wasN position in the ring. Table 4 presents a list of effective quantum chemical parameters in the evaluation of corrosion inhibitors.

Table 4. Quantum chemical parameters for NTA and $NTAH^+$in gas (g) and aqueous (aq) phases

Inhibitor form	Phase	E_{HOMO} (eV)	E_{LUMO} (eV)	ΔE_g(eV)	η(eV)	P (D)	ω(eV)
NTA	aq	-5.89	-1.64	4.24	2.12	2.46	1.67
	g	-5.74	-1.44	4.30	2.15	1.85	1.50
$NTAH^+$	aq	-6.50	-1.98	4.51	2.25	11.48	1.99
	g	-9.27	-5.37	3.89	1.94	8.31	6.88

The E_{HOMO} (highest occupied molecular orbital energy) value indicates the electron donating ability of the inhibitor. Thus, the higher value of E_{HOMO} shows an increasing interaction of the inhibitor with metal, while E_{LUMO} (the lowest unoccupied molecular orbital energy) implies the electron-accepting ability of the inhibitor. As a result, we may argue that the decrease of E_{LUMO} of inhibitor is an indication of the increase of electron-accepting ability of the inhibitor from electrons of 3d orbitals of the metal. Therefore, the lower value of ΔE_g indicates the higher inhibition efficiency of the inhibitors. According to Table 4, the calculated value of E_{LUMO} for $NTAH^+$ in both gas and aqueous phases is lower than that of NTA, indicating the higher interaction of the $NTAH^+$ with metal and its higher inhibition efficiency. Value of ΔE_g in gas for the protonated form of inhibitor is detected to be lower than the non-protonated form of inhibitor, indicating that protonated form is more reactive than the non-protonated form. Moreover, values of ΔE_g in thegas phase are lower than the aqueous phase. So, we may conclude that the presence of solvent can affect molecular properties.

Electron affinity (A) and ionization potential (I) of the molecules could be calculated through the following equations [54,55]:

$$A = -E_{LUMO} \quad (9)$$

$$I = -E_{HOMO} \quad (10)$$

Applying the following equations, we can measure global hardness (η) and chemical potential (μ) through I and A[56–58]:

$$\eta = \frac{I-A}{2} \quad (11)$$

$$\mu = -\frac{A+I}{2} \quad (12)$$

η is an effective parameter in molecular reactivity and stability. The lower values of global hardness are expected to result in the higher ability of the inhibitor for donating the electron to metal and better adsorption of inhibitor on the surface of metal. Based on the values of η in Table 4, $NTAH^+$ in gas phase has lowest hardness in investigated cases, which indicates the better adsorption of $NTAH^+$ in gas phase comparison with NTA.

Dipole moment (P) is the measure of the polarity of a polar covalent bond, and the total dipole moment for a molecule is the vector sum of individual bond dipole moments [59,60].Any increase in the value of P can result in further adsorption on the metal [61]. Table 4 reveals that values of the P for $NTAH^+$ are higher than NTA. The results suggest that the better adsorption in protonated form as compared with non-protonated form. Moreover, values of the P are found to be more in the aqueous phase than the gas phase. So, the presence of solvent can increase the deformation of the inhibitor. Electrophilicity (ω), the electron-accepting capability of a molecule, can be acquired through η and μ by using the following equation [56,62,63]:

$$\omega = \frac{\mu^2}{4\eta} \quad (13)$$

Table 4 shows that in all examined cases, values of ω for $NTAH^+$ are higher than those of NTA, indicating that electron-accepting capability of $NTAH^+$ from the metal is higher than that of NTA. Figure10 illustrates HOMO and LUMO density distributions on the NTA and $NTAH^+$. According to this figure, HOMO in NTA and $NTAH^+$ in gas and aqueous phases is mostly localized on S and also distributed on over C=C double bonds of the thiazol ring, and the amine group. Thus, these sites are probably for interacting with metal and donating electron.LUMO distribution is mostly localized at naphthalene ring. Hence, these sites are detected to be suitable for feedback bonds with metal [64].

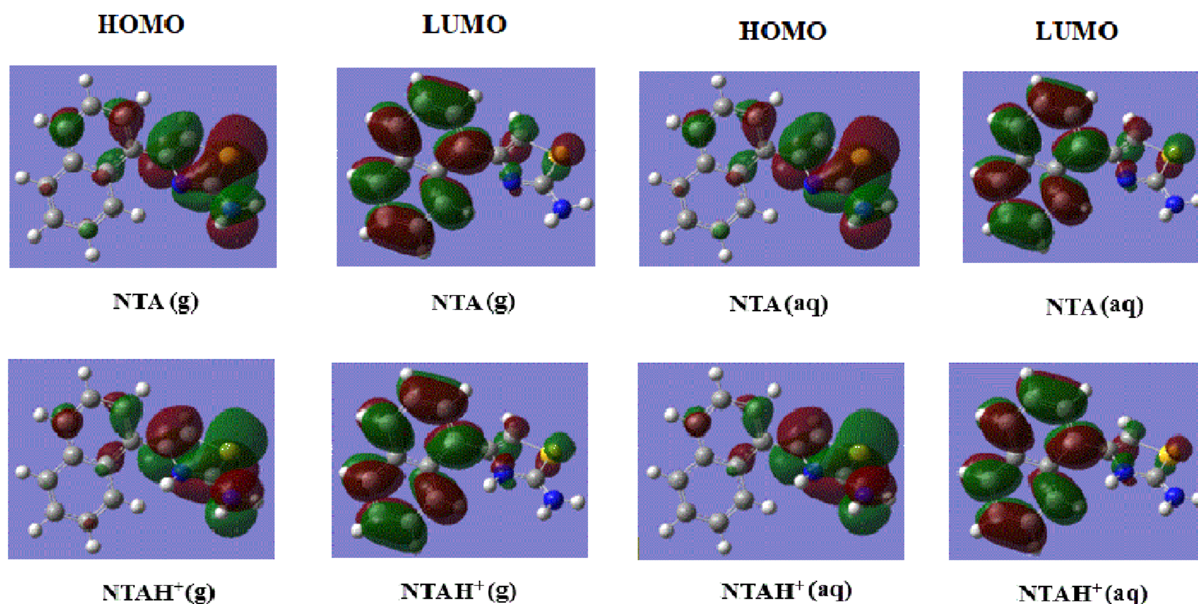

Figure 10. The frontier molecular orbitals distribution of the NTA and $NTAH^+$ in the gas (g) and the aqueous(aq) phases.

Adsorption of NTA and $NTAH^+$ on the copper surface has been investigated by MD simulation and quantum calculations. Figures 11 and 12show the final structure of MD simulation and quantum calculations, respectively. In the MD simulation, the energy and temperature of the system reached to the equilibrium state. As shown in Figure 11, it can be seen that NTA and $NTAH^+$ have parallel adsorption mode. The values of E_{int} between the metal and inhibitor from MD simulation and quantum calculations are summarized in Table 5. Results show that $NTAH^+$ has more negative E_{int} value and stronger interactions with the copperin comparison withNTA. This result can be attributed tothe electrostatic reaction with metal surface in addition interaction via π electrons of rings and lone pair electrons in N with copper.

Table 5. The obtained interaction energies for NTA and $NTAH^+$ with Cu surface by using quantum calculations and MD simulation.

System	E_{int} (kJ mol^{-1})	
	quantum calculations	MD simulation
$NTAH^+$/Cu	-99.27	-117.75
NTA/Cu	-97.23	-94.29

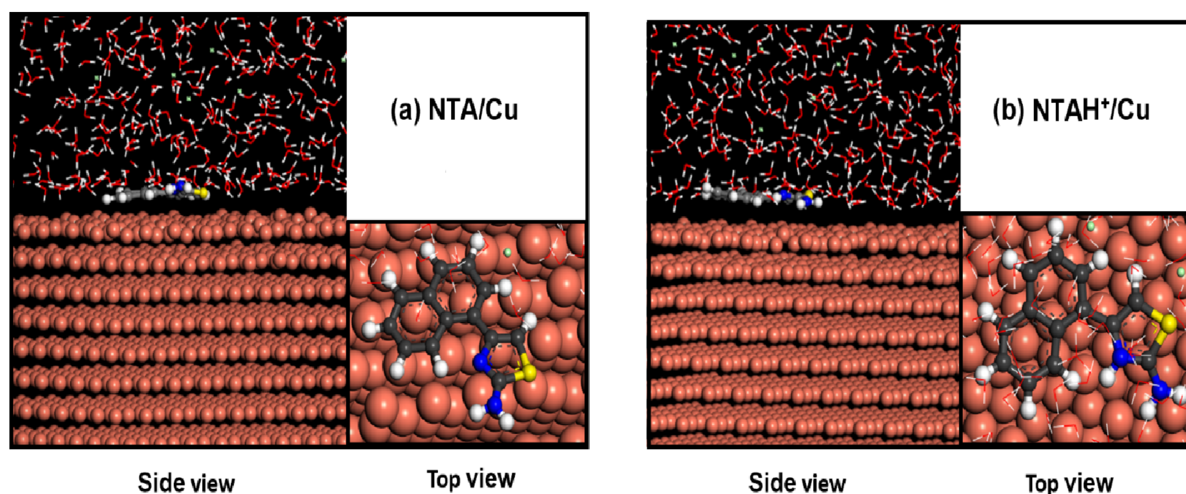

Figure 11. The Equilibrium adsorption geometries of (a) NTA and (b) $NTAH^+$ on Cu (111) surface (side and top views).

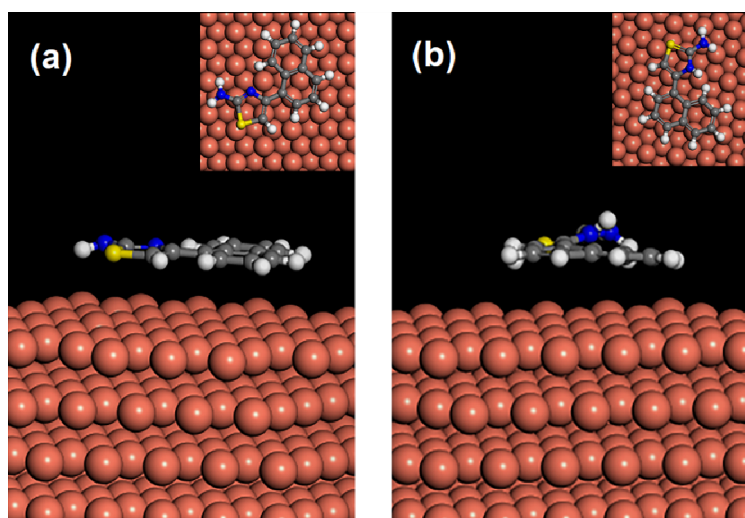

Figure 12. Optimized adsorption geometries of (a) NTA and (b) $NTAH^+$ on Cu (111) surface from quantum calculations (side and top views).

Conclusions

1- The copper corrosion inhibition efficiency of NTA at optimum concentration was about 90%; hence, this compound can be employed as an effective corrosion inhibitor.

2- In the present study, the maximum shift in E_{corr} value in the presence of the inhibitor compared with the blank solution was less than 85 mV, suggesting that the NTA is a mixed-type inhibitor; however, in the presence of NTA significantly affected the cathodic reaction.

3- The adsorption of the studied NTA obeys the Langmuir adsorption isotherm. ΔG^0_{ads} values for this compound were between -20 to -40 kJ mol^{-1}, indicating the occurrence of physical and chemical adsorption.

4- The phase graph shows two maximums, indicating two time constants for two occurring processes on the surface.

5- The results of EIS and Tafel tests were in agreement with the results of surface analyses.

6- $NTAH^+$ had more negative E_{int} value and stronger interactions with the copper surface in comparison with NTA.

Acknowledgment

We appreciatethe Research Council of the Iran University of Science and Technology for their partial contribution in this study.

References

[1] B. Duran, G. Bereket, M. Duran, *Prog. Org. Coatings*., 73, 162 (2012).

[2] E.M. Sherif, *Int. J. Electrochem. Sci*., 7, 1884 (2012).

[3]B.A. Abd-El-Nabey, A.H. Abdel-Gaber, M.E.S. Ali, E. Khamis, S. El-Housseiny, Int. *J. Electrochem. Sci.,* 8, 7124 (2013).

[4] D. Wang, B. Xiang, Y. Liang, S. Song, C. Liu, *Corros. Sci*., 85, 77 (2014).

[5] A. Fateh, M. Aliofkhazraei, A.R. Rezvanian, *Arab. J. Chem*., in press (2017).

[6] W. Gong, X. Yin, Y. Liu, Y. Chen, W. Yang, *Prog. Org. Coatings*, 126, 150 (2019).

[7] R. Farahati, A. Ghaffarinejad, H. (Jafar) Rezania, S.M. Mousavi-Khoshdel, H. Behzadi, *Colloids Surfaces A*., 578, 123626 (2019).

[8] M.B. Petrovi, M.B. Radovanovi, Ž.Z. Tasi, M.M. Antonijevi, *J. Mol. Liq*., 225, 127 (2017).

[9] M. Yadav, D. Behera, S. Kumar, R.R. Sinha, *Ind. Eng. Chem. Res*., 52, 6318 (2013).

[10] M.L. Zheludkevich, K.A. Yasakau, *Corros. Sci*., 47, 3368 (2005).

[11] G. Wells, T.D. Bradshaw, P. Diana, A. Seaton, D. Shi, A.D. Westwell, M.F.G. Stevens,*Bioorg. Med. Chem. Lett*., 10, 513 (2000).

[12] S.R. Pattan, C. Suresh, V.D. Pujar, V.V.K. Reddy, V.P. Rasal, B.C. Koti, *Indian J. Chem*., 44, 2404 (2005).

[13] Y. Kumar, R. Green, D.S. Wise, L.L. Wotring, L.B. Townsend, *J. Med. Chem*., 36, 3849 (1993).

[14] S. Rollas, S.G. Küçükgüzel, *Molecule*s, 12, 1910 (2007).

[15] A.A. Chavan, N.R. Pai, *Arkivoc.,*16, 148 (2007).

[16] X.F. Liu, S.J. Huang, H.C. Gu, *Int. J. Fatigue*., 24, 803 (2002).

[17] A. Döner, R. Solmaz, M. Özcan, G. Kardaş, *Corros. Sci*., 53, 2902 (2011).

[18] A.A. Al-Sarawya, A.S. Foudab, W.A. Shehab El-Deina, *Desal*., 229, 279 (2008).

[19] L. Guo, X. Ren, Y. Zhou, S. Xu, Y. Gong, S. Zhang, *Arab. J. Chem*., 10, 121 (2017).

[20] S. Kaya, C. Kaya, L. Guo, F. Kandemirli, B. Tüzün, İ. Uğurlu, L.H. Madkour, M. Saraçoğlu, *J. Mol. Liq*., 219, 497 (2016).

[21] R. Farahati, A. Ghaffarinejad, S.M. Mousavi-Khoshdela, J. Rezania, H. Behzadi, A. Shockravi, *Prog. Org. Coatings*., 132, 417 (2019).

[22] I.H.R. Tomi, A.H.R. Al-Daraji, S.A. Aziz, Synth. *React. Inorganic, Met. Nano-Metal Chem*., 45, 605 (2015).

[23] S. Mo, H.Q. Luo, N.B. Li, J. *Colloid Interface Sci.*, 505, 929 (2017).

[24] S. Chen, B. Xiang, S. Chen, X. Zou, Y. Zhou, J. Hou, *Appl. Surf.* Sci., 456, 25 (2018).

[25] D. Chadwick, T. Hashemi, *Surf. Sci*., 89, 649 (1979).

[26] J. Rezania, H. Behzadi, A. Shockravi, M. Ehsani, E. Akbarzadeh, *J. Mol. Struct*., 1157 300 (2018).

[27] A.D. Becke, *J. Chem. Phys.,*98, 5648 (1993).

[28] A.D. Becke, *Phys. Rev. A.,* 38, 3098 (1988).

[29] C. Lee, W. Yang, R.G. *Parr, Phys. Rev. B.*, 37, 785 (1988).

[30] M.J. Frisch, et al., Gaussian 03, Revision C.02, Gaussian, Inc., Wallingford CT, (2004).

[31] Materials Studio, Revision 6.0, Accelrys Inc., San Diego, USA, (2011).

[32] H. Sun, *J. Phys. Chem. B*., 5647, 7338 (1998).

[33] S. Kaya, P. Banerjee, S.K. Saha, B. Tüzün, C. Kaya, *RSC Adv*., 6, 74550 (2016).

[34]E. Kowsari, S.Y. Arman, M.H. Shahini, H. Zandi, A. Ehsani, R. Naderi, A. Pourghasemi-Hanza, M. Mehdipour, *Corros. Sci*., 112, 73 (2016).

[35] C. Bhan, M.A. Quraishi, A. Singh, *J. Taiwan Inst. Chem. Eng*., 49, 229 (2015).

[36] Y. Peng, A.E. Hughes, G.B. Deacon, P.C. Junk, B.R.W. Hinton, M. Forsyth, J.I. Mardel, A.E. Somers, *Corros. Sci*., 145, 199 (2018).

[37] C. Rahal, M. Masmoudi, R. Abdelhedi, R. Sabot, M. Jeannin, M. Bouaziz, P. Refait, *J. Electroanal. Chem*., 769, 53 (2016).

[38] D. Zhang, Q. Cai, X. He, L. Gao, G. Zhou, *Mater.Chem. Phys*., 112, 353 (2008).

[39] E.M. Sherif, R.M. Erasmus, J.D. Comins, *J. Colloid Interface Sci*., 311, 144 (2007).

[40] Q. Ma, S. Qi, X. He, Y. Tang, G. Lu, *Corros. Sci*., 129, 91 (2017).

[41] X. Ma, L. Xu, W. Wang, Z. Lin, X. Li, *Corros. Sci*., 120, 139 (2017).

[42] B. Tan, S. Zhang, Y. Qiang, L. Guo, L. Feng, C. Liao, Y. Xu, S. Chen, *J. Colloid Interface Sci*., 526, 268 (2018).

[43] R. Salahandish, A. Ghaffarinejad, A. Moradpour, *J. Appl. Chem. Res*., 10, 97 (2016).

[44] M. Mehdipour, R. Naderi, B.P. Markhali, *Prog. Org. Coatings*., 77, 1761 (2014).

[45] M.A. Amin, K.F. Khaled, Q. Mohsen, H.A. Arida, *Corros. Sci*., 52 (2010).

[46] K. Azzaoui, E. Mejdoubi, S. Jodeh, A. Lamhamdi, E. Rodriguez-Castellón, M. Algarra, A. Zarrouk, A. Errich, R. Salghi, H. Lgaz, *Corros. Sci*., 129, 70 (2017).

[47] F. El-Taib Heakal, M.A. Deyab, M.M. Osman, M.I. Nessim, A.E. Elkholy, *RSC Adv*., 7, 47335 (2017).

[48] K. Zhang, B. Xu, W. Yang, X. Yin, Y. Liu, Y. Chen, *Corros. Sci*., 90, 284 (2015).

[49] Y. Qiang, S. Zhang, S. Yan, X. Zou, S. Chen, *Corros. Sci*., 126, 295 (2017).

[50] J. Haque, K.R. Ansari, V. Srivastava, M.A. Quraishi, I.B. Obot, *J. Ind. Eng. Chem*., 49, 176 (2017).

[51] B.P. Charitha, P. Rao, *J. Ind. Eng. Chem*., 58, 357 (2018).

[52] M. Mobin, M. Rizvi, *Carbohydr. Polym*., 160, 172 (2017).

[53] Y. Guo, B. Xu, Y. Liu, W. Yang, X. Yin, Y. Chen, J. Le, Z. Chen, *J. Ind. Eng. Chem*., 56, 234 (2017).

[54] J.P. Perdew, R.G. Parr, M. Levy, J.L. Balduz, *Phys. Rev. Lett*., 49, 1691 (1982).

[55] M.L. John P. Perdew, *Phys. Rev. B*., 56, 16021 (1997).

[56] R.G. Parr, L. V. Szentpály, S. Liu, *J. Am. Chem. Soc*., 121, 1922 (1999).

[57] A.S. Fouda, M.A. Ismail, A.S. Abousalem, G.Y. Elewady, *RSC Adv*., 7, 46414 (2017).

[58] S. Kaya, P. Banerjee, S.K. Saha, B. Tüzün, C. Kaya, *RSC Adv*., 6, 74550 (2016).

[59] O. Kikuchi, *Mol. Inform*., 6, 179 (1987).

[60] G. Gece, *Corros. Sci*., 50, 2981 (2008).

[61] N.A. Wazzan, *J. Ind. Eng. Chem.*, 26, 291 (2015).

[62] A. Kokalj, *Electrochim. Acta*., 56, 745 (2010).

[63] I.B. Obot, Z.M. Gasem, *Corros. Sci.*, 83, 359 (2014).

[64] M. Shahraki, M. Dehdab, S. Elmi, J. *Taiwan Inst. Chem. Eng.*, 62, 313 (2015).